Journal of
Composites Science

MDPI

Article

Influence of Cutting Speed during the Turning of Inconel 718 on Oxidation Wear Pattern on the Zr-ZrN-(Zr,Mo,Al)N Composite Nanostructured Coating

Alexey Vereschaka [1,*], Filipp Milovich [2], Nikolay Andreev [2], Mars Migranov [3], Islam Alexandrov [1], Alexander Muranov [1], Maxim Mikhailov [1] and Aslan Tatarkanov [1]

[1] Institute of Design and Technological Informatics of the Russian Academy of Sciences (IDTI RAS), Moscow 127055, Russia
[2] Materials Science and Metallurgy Shared Use Research and Development Center, National University of Science and Technology MISiS, Moscow 119049, Russia
[3] VTO Department, Moscow State Technological University STANKIN, Moscow 127055, Russia
* Correspondence: dr.a.veres@yandex.ru

Abstract: The properties and oxidation wear patterns in the composite nanostructured coating of Zr-ZrN-(Zr,Mo,Al)N were studied during the turning of Inconel 718 alloy at the cutting speeds of v_c = 125 and 200 m/min. The hardness of the coating, its elastic modulus, and critical fracture load during the scratch testing were determined. The study focused on the tribological properties of the Zr-ZrN-(Zr,Mo,Al)N coating at temperatures of 400–900 °C paired with an insert made of Inconel 718, which exhibited a certain advantage over the reference coatings of Zr-ZrN and Ti-TiN-(Ti,Cr,Al)N of similar thickness. The coating of Zr-ZrN-(Zr,Mo,Al)N provided for the longest tool life at the cutting speed of v_c = 125 m/min (the tool life was four times longer in comparison with that of the uncoated tool and 15% longer in comparison with that of the Ti-TiN-(Ti,Cr,Al)N-coated tool) and at the cutting speed of v_c = 200 m/min (the tool life was 2.5 times longer in comparison with that of the uncoated tool and 75% longer in comparison with that of the Ti-TiN-(Ti,Cr,Al)N-coated tool). While at the cutting speed of v_c = 125 m/min, the surface coating layers exhibit only partial oxidation of the external layers (to a depth not exceeding 250 nm), with mostly preserved cubic nitride phases, and then the cutting speed of v_c = 200 m/min leads to almost complete oxidation (to the depth of at least 500 nm), however, with a partially preserved nanolayered structure of the coating.

Keywords: Inconel 718; multilayer nanocomposite coatings; wear resistance; turning; wear mechanism; cutting speed

Citation: Vereschaka, A.; Milovich, F.; Andreev, N.; Migranov, M.; Alexandrov, I.; Muranov, A.; Mikhailov, M.; Tatarkanov, A. Influence of Cutting Speed during the Turning of Inconel 718 on Oxidation Wear Pattern on the Zr-ZrN-(Zr,Mo,Al)N Composite Nanostructured Coating. *J. Compos. Sci.* **2023**, *7*, 18. https://doi.org/10.3390/jcs7010018

Academic Editor: Prashanth Konda Gokuldoss

Received: 15 November 2022
Revised: 9 December 2022
Accepted: 3 January 2023
Published: 6 January 2023

1. Introduction

Inconel 718 is an austenitic nickel–chromium heat-resistant alloy used for the manufacturing of products to be operated at temperatures reaching 700 °C [1–3]. Due to its excellent performance properties, Inconel 718 is one of the most widely used alloys of the Inconel family. Inconel 718 contains nickel (Ni, 50.0–55.0%), iron (Fe, 18–20%), chromium (Cr, 17.0–21.0%), niobium (Nb, 4.75–5.50%), molybdenum (Mo, 2.80–3.30%), and tungsten (W, 2.50–3.50%). The presence of small amounts (not exceeding 1%) of aluminum (Al), manganese (Mn), and silicon (Si) may also be detected [1–3].

The machining of products made of Inconel 718 alloy is accompanied with some difficulties arising due to its low thermal conductivity, inhibiting the removal of heat from the cutting zone [4–6]. Therefore, high temperature in the cutting zone is a key challenge during the cutting of Inconel 718. Furthermore, Inconel 718 exhibits work hardening during the machining, and its structure may contain hard carbide grains that have an abrasive effect on cutting tools. In addition to the above-mentioned factors, Inconel 718 is a considerably hard material, also prone to high adhesion to the tool material. Another factor

hindering the machining of the products made of Inconel 718 is the intense interdiffusion interaction with the external layers of the tool material at elevated temperatures in the cutting zone. Thus, Inconel 718 is a hard-to-cut material, machined at considerably low cutting speeds (not exceeding 100 m/min) in order to reduce the wear rate of the cutting tools [7–17]. The cutting speed may be significantly increased (up to 200 m/min) due to the use of coated tools [18–20]. For an uncoated tool, the temperature in the cutting zone already reaches 1000 °C at the cutting speed of v_c = 35 m/min [6], and for a coated tool, the temperature of 1000 °C is typical for the cutting speed of v_c = 100 m/min [18]. The analysis focused on the composition of the coatings used during the cutting of Inconel 718 proves the dominance of the systems of TiN, TiCN, and TiAlN [7–18]. Several papers [4,7,17] have considered the alternative systems of CrN [10,21] and Al_2O_3.

2. Rationale for the Choice of Coating Composition

The machining of Inconel 718 is highly influenced by the oxidation and diffusion wear mechanisms [18–20]. In the conditions of the mentioned wear mechanisms, the use of the coatings containing such elements as molybdenum (Mo) and aluminum (Al) [22–25] is advisable. These elements ensure the formation of Al_2O_3- and MoO_2-based protective tribological oxide films [26–28]. At the same time, the mentioned cutting conditions are usually accompanied with noticeable thermal and mechanical loads, which cause active cracking in the structure of the coatings [29–32]. From this point of view, it is also reasonable to use the coatings based on the ZrN system that are not only characterized by enhanced resistance to cracking but also form oxide grains of ZrO_2 at elevated temperatures, which have a positive effect on the tribological conditions in the cutting zone [33]. Thus, with the introduction of such elements as Mo and Al, the ZrN-based coating may be effective during the machining of Inconel 718.

A texture with the orientation of (111) is typical for the ZrN system [34]. Several papers [35–37] note that the introduction of aluminum (Al) into the coating composition enhances such properties of the coatings as hardness and wear resistance combined with heat resistance. When Al is introduced in the composition of the ZrN system, the texture of the coating decreases, and the orientations of (200) and (220) are also formed [34]. The presence of Al in the coating composition provides an increase in its hardness (from 21 to 28 GPa). When the content of Al is relatively low, a cubic phase of c-(Zr,Al)N, characterized by high hardness (about 35 GPa), is formed in the coating. However, with an increase in the content of Al, a hexagonal phase of h-(Zr,Al)N, characterized by significantly low hardness (about 20 GPa) and wear resistance, is formed [38]. The cubic structure has a lower heat resistance in comparison with the hexagonal one [39,40]. Therefore, the introduction of Al into the ZrN system leads to the formation of solid solution and distortion of crystal lattice, which enhances hardness, wear resistance, and thermal stability of the coatings. A positive tribological and protective effect is also produced by the formation of Al_2O_3 oxide on the surfaces of the coatings containing Al [41].

The influence of the percentage of the Al content on the properties of the (Zr,Al)N coating was investigated. In particular, when the content of Al is 36 at%, the hardness of the coating is 36 GPa [42]. In this case, the hardness of the (Zr,Al)N coating (like the hardness of the other coatings) substantially depends on the deposition condition and the technique of measurement. For example, in [34], it is noted that when the content of Al grows up to 43 at%, the hardness of the (Zr,Al)N coating increases from 21 to 28 GPa. In [34], the studies detected in the coating only the fcc phase of (Zr,Al)N. According to the other data, the hexagonal phase begins to form when the Al content is 36 at% and higher, a mixture of hexagonal and cubic phases is detected when the Al content is 36–70 at%, and only a hexagonal phase is observed when the Al content exceeds 70 at% [38]. Similar data are contained in [40]. However, there are also data that the hexagonal phase of h-AlN is already being formed when the coating contains 34 at% Al [43].

The phase composition of the coating is significantly influenced by temperature. In particular, when the (Zr,Al)N coating is heated up to 800 °C, recrystallization occurs upon

diffusion of nitrogen from the fcc phase. This process leads to a decrease in the hardness and wear resistance of the coating [38]. In general, the c-(Zr,Al)N phase remains stable at temperatures up to 1000 °C, but higher temperatures cause active decomposition of the cubic phase and formation of h-AlN. It is found that coatings with higher content of Al are characterized by higher thermal stability [39]. At temperatures of 1000 °C and higher, the coatings with higher content of Al exhibit the decomposition of the h-(Zr,Al)N hexagonal phase with the formation of grains of the c-ZrN cubic phase due to the diffusion of zirconium. When heated up to 1150 °C, the coating with 34 at% Al demonstrates active formation of cubic structures with high content of Zr and simultaneous growth of (semi-) coherent phases of AlN [43]. At temperatures above 1150 °C, no coherence is detected, but the hardness stays at the level of 29 GPa. At the same time, the coating with 32 at% Al forms the incoherent structure of h-AlN only at temperatures above 1270 °C, and the hardness of the coating stays at the level of 33 GPa [43]. The coating oxidizes upon being heated in the oxygen-containing atmosphere. The oxidation resistance of the coating enhances with the increase in the Al content from 15 to 58 at% and can reach 800 °C [44]. In this case, the coating exhibits the formation of ZrO_2 zirconium oxide, and the formation of Al_2O_3 aluminum oxide is detected only at temperatures above 900 °C. However, the highest wear resistance of the cutting tools was ensured by the coating with 15 at% Al [44].

The introduction of molybdenum (Mo) in the composition of the coatings can have a significant positive effect on their properties. The coating of (Mo,Al)N is characterized by high hardness (32.6–38.4 GPa) [45–48]. In this system, the fcc phase continues to dominate when the content of Al is below 65 at.% [47]. When the content of Al is higher, a hexagonal phase is being formed, which decreases the hardness of the coating to 22 GPa [47]. With a growth in the Al content, the process of active oxidation begins at higher temperature, which reaches 700 °C at 33 at.% Al [48]. At the same time, the growth in the Al content leads to an increase in grain sizes and a slight decrease in the strength of the coating [48].

The coatings that contain Zr, Al, and Mo simultaneously are characterized by good mechanical and performance properties, often superior to the properties of the (Zr,Al)N or (Mo,Al)N coatings [45–49]. It is found that the (Zr,Al,Mo)N coating with the similar content of Zr and Mo forms two fcc phases: ZrN and MoN [49–52]. The hardness of the (Zr,Al,Mo)N coating reaches 27–30 GPa [49]. The presence of molybdenum contributes to a noticeable decrease in the coefficient of friction (COF) at temperatures above 500 °C [49–51].

During the turning of steel with a (Zr1−x,Alx)N-coated tool (where x = 0, 0.35, 0.50, or 0.83) at the cutting speeds of v_c = 220 and 240 m/min, the abrasive and adhesive-fatigue wear mechanisms prevail, with no noticeable signs of oxidation wear [53]. However, during the turning of Inconel 718 alloy, it is the oxidation and diffusion factors that become significant [18–20]. Thus, the best choice would be the coating that effectively resists both abrasive and adhesive-fatigue (cracking) wear and exhibits good resistance to oxidation and diffusion.

Therefore, the coating of Zr-ZrN-(Zr,Mo,Al)N was chosen for the study, since this system combines considerably high hardness and wear resistance with sufficient strength and resistance to cracking. It is also assumed that this coating will have high heat resistance, and aluminum and molybdenum oxides formed on its surface at elevated temperatures will have a positive effect on the tribological parameters in the cutting zone [41,44,49–51]. The coatings of Zr-ZrN and Ti-TiN-(Ti,Cr,Al)N were chosen as objects of comparison, as the coatings based on (Ti,Al)N and (Ti,Cr,Al)N are actively used in the machining of Inconel 718. The coating of Zr-ZrN, like the coating of Zr-ZrN-(Zr,Mo,Al)N, is built on the basis of the cubic phase of c-ZrN, but with no Mo and Al introduced in the coating composition. The coatings of Zr-ZrN-(Zr,Mo,Al)N and Ti-TiN-(Ti,Cr,Al)N have a three-layer architecture, including an adhesive layer (Zr or Ti, respectively, 20–50 nm thick), a transition layer (ZrN or TiN, respectively, 500–900 nm thick), and a wear-resistant layer ((Zr,Mo,Al)N or (Ti,Cr,Al)N, respectively, 500–900 nm thick). The choice of parameters for a three-layer architecture is substantiated in [54–56]. The Zr-ZrN coating has only an adhesive layer of Zr, about 40 nm thick, with the total coating thickness reaching 5 μm.

For convenience, the coatings under consideration will be further designated by the composition of their wear-resistant layers: ZrN, (Zr,Mo,Al)N, or (Ti,Cr,Al)N, respectively.

3. Materials and Methods

The coatings under consideration were deposited on samples using the VIT-2 special unit (IDTI RAS-MSTU STANKIN, Moscow, Russia). This unit implements the upgraded technology of physical vapor deposition (PVD) and is able to generate coatings of a wide range of compositions and structures [57–61]. The VIT-2 unit is equipped with evaporators of two systems, including the evaporator of controlled accelerated arc (CAA-PVD) [60,61] and the evaporator of the filtered cathodic vacuum arc deposition (FCVAD) [57–59]. A cathode of Al (99.8%) was installed on a cathode unit of the FCVAD system, and, depending on the type of the coating to be deposited, cathodes of Zr (99.8%), Mo (99.8%), Cr (99.9%), and Ti (99.6%) were installed on a cathode unit of the CAA-PVD system.

Before the deposition of the coatings, the samples were washed in the specially prepared active solution using ultrasonic stimulation. Then, the samples were washed in purified water and dried in a stream of warm purified air.

Before the coating deposition, the samples placed in the chamber underwent the procedure of cleaning and thermal activation in the gas and metal plasma flow in the following conditions: gas (Ar) pressure 2.0 Pa, voltage on substrate 110 V.

During the deposition of the coatings, the cathode arc current was 110 A, 75 A, 140 A, 160 A, and 110 A, respectively, for the cathodes of Zr, Cr, Mo, Al, and Ti at voltage on substrate −150 V.

At various stages of coating deposition, the following nitrogen pressure (pN) in the chamber was maintained:

Pumping and heating of vacuum chamber: p_N = 0.06 Pa.
Heating and cleaning of products with gaseous plasma: p_N = 2.00 Pa.
Deposition of coating: p_N = 0.42 Pa.
Cooling of products: p_N = 0.06 Pa.
The surface temperature of the samples was 650–700 °C.

The turntable rotation speed was n = 0.7 rpm, which provides for the formation of a coating with the modulation period of about 50 nm [31].

The coatings were deposited using square-shaped carbide cutting inserts without a hole (SNUN ISO 1832:2012). The inserts were made of (WC + 15% TiC + 6% Co) carbide. Cylindrical indenters with hemispherical ends were made to carry out tribological tests. The material of the indenters was identical to the material of cutting inserts (WC + 15% TiC + 6% Co). The coatings for the cutting inserts and the indenter were deposited during the same technology cycle, which ensured the identity of the coating parameters.

A transmission electron microscope (TEM) of JEM 2100 (JEOL, Tokyo, Japan) was used to study the structure of the coatings. The accelerating voltage of 200 kV was applied. The TEM with the EDX (energy-dispersive X-ray spectroscopy) system INCA Energy (OXFORD Instruments, Abingdon, UK) was used. Cross-sections (lamellas) for the testing were made with a Strata focused ion beam (FIB) 205 (FEI, USA). A scanning electron microscope (SEM) of FEI Quanta 600 FEG was also used to study the coating structure.

A mechanical tester of CB-500 (Nanovea, Irvine, CA, USA) with a nanomodule was used to measure hardness and elastic modulus. The measurement was carried out at the maximum load of 200 mN and the loading rate of 400 mN/min.

The methods of L. Sh. Shuster [55–58,62] were applied to study the tribological properties of the samples. The investigation was carried out with the special equipment to determine the tribological parameters at the temperatures not exceeding 1000 °C and the pressures corresponding to the conditions in the cutting zone. The measurements were carried out in an "indenter-insert" pair, in which the indenter simulated a coated cutting tool, and the insert was made of Inconel 718. The following parameters were determined:

- Adhesive bond strength τ_{nn}.

- Value of normal stresses Prn acting on the surface of the indenter.

The value of the adhesion component of the COF fadh was determined by the formula:

$$f_{adh} = \frac{\tau_n}{p_r}$$

The cutting properties and wear resistance of the coated and uncoated samples during the turning of Inconel 718 were studied on a CU 500 MRD lathe (Sliven) with a ZMM CU 500 MRD variable-speed drive. The cutting geometry parameters were as follows: $\gamma = -7^\circ$, $\alpha = 7^\circ$, $\lambda = 0$, r = 0.4 mm, with the cutting conditions as follows: f = 0.1 rpm, a_p = 0.5 mm, and v_c = 125 and 200 m/min.

The flank wear of VB_{max} = 0.3 mm was used as the limit wear criterion. To plot the "flank wear-cutting time" relationship curves, the following techniques were used. Five tests were carried out for the samples with each type of the coatings and for the uncoated sample. The cutting process was interrupted at regular intervals to measure the wear rate with the optical microscope. Based on the obtained data, the average wear value was determined for each time interval. The curve also exhibited scatter of wear rate values (with the help of the corresponding error bars). For the metallographic studies, a sample was subjected to continuous cutting (the cutting process was not stopped) to obtain an adequate picture of wear and oxidation processes.

4. Results

4.1. Comparison of the Properties of the Coatings under Consideration

Table 1 presents the measurement results concerning the hardness, elastic modulus, and critical fracture load of the coatings. The (Ti,Cr,Al)N and (Zr,Mo,Al)N coatings are characterized by close, almost identical hardness, while the ZrN coating exhibits noticeably lower hardness. It should be noted that the presented data concerning the hardness values were obtained at room temperature. In the conditions of the cutting zone, the temperature can reach 800–1000 °C, and in these conditions, the coating hardness values will differ considerably from the values measured at room temperature. The value of the critical fracture load L_{C2} of all three coatings has a slightly different meaning for monolithic and multilayered coatings: while for the monolithic coatings this value mainly describes the strength of the adhesive bond to the substrate, for the multilayered coatings, the strength of the coherent bond between the layers is also important. In any case, a certain value of L_{C2} is quite high and may indicate both good adhesion to the substrate and the strong cohesive bonds between the coating nanolayers.

Table 1. Hardness, elastic modulus, and critical fracture load of the coatings.

Coating	Hardness, GPa	Elastic Modulus, GPa	Critical Fracture Load L_{C2}, N
ZrN	27.3 ± 1.5	321.7 ± 23.6	>40
(Ti,Cr,Al)N	31.9 ± 1.4	580.5 ± 22.4	38
(Zr,Mo,Al)N	32.3 ± 1.2	432.1 ± 21.4	>40

The analysis of the chemical composition of the coatings exhibits almost identical content of Al in the coatings of (Ti,Cr,Al)N and (Zr,Mo,Al)N (12.4 and 13.3 at.%, respectively). There is a similarity in the percentage of metal content within the pairs of Ti and Zr (49.3 and 51.7 at%, respectively), on the one hand, and Cr and Mo (38.3 and 35.0 at%, respectively), on the other hand.

The ZrN coating has a monolithic structure, with average grain sizes of 200–500 nm (Figure 1a). The coatings of (Ti,Cr,Al)N and (Zr,Mo,Al)N have a nanolayered structure with the modulation periods of 45 and 48 nm, respectively (Figure 1b,c). The total thickness of each of the considered coatings reaches about 5 μm.

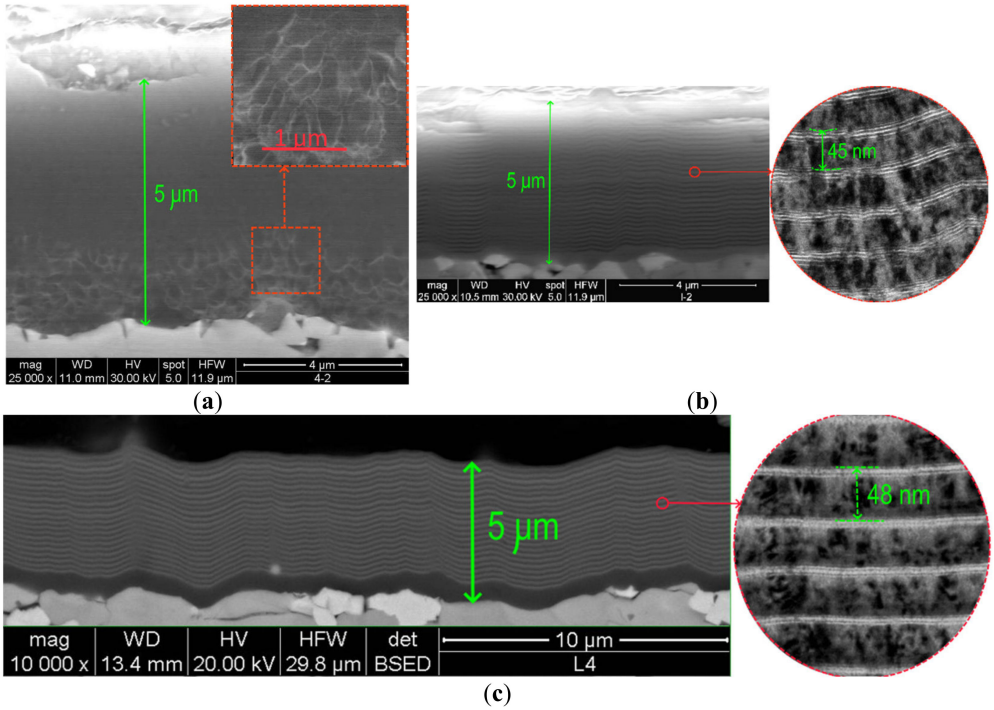

Figure 1. Structure of the coatings: (**a**) ZrN, (**b**) Ti-TiN-(Ti,Cr,Al)N, and (**a**) Zr-ZrN-(Zr,Mo,Al)N. SEM, except for the high-resolution (HR) images of the coating structures on (**b**,**c**) obtained using TEM. Due to the difference between the SEM and TEM techniques and the different resolutions of the corresponding images, the SEM image exhibits only the alternation of the modulation periods, while the TEM image demonstrates the features of the nanolayered structure of the coatings.

The analysis of the phase composition of the coatings, conducted using the X-ray diffraction (XRD) technique, finds the presence of one dominant fcc phase for each of the three coatings under consideration (Figure 2). These are phases of c-ZrN, c-(Ti,Cr,Al)N, and c-(Zr,Mo,Al)N, respectively. The coating of (Ti,Cr,Al)N also contains a phase of metallic chromium, which may be explained due to the presence of Cr microparticles on the coating surface.

The studies of the tribological properties of the coatings under consideration prove there are noticeable differences in the change in these properties for various coatings depending on temperatures (Figure 3). Given the shear strength of adhesive bonds τnn, the most favorable properties are detected for the coating of (Zr,Mo,Al)N, which also exhibits the maximum value of normal stresses Prn, which characterizes the deformation component of friction. As a result, the coating of (Zr,Mo,Al)N has the minimum value of the adhesion component of the COF fadh over the entire temperature range under consideration. The coating of (Ti,Cr,Al)N exhibits high values of the shear strength of adhesive bonds τnn. The studies are carried out for the tribological pairs, in which the contacting material is Inconel 718 alloy, containing a significant amount of chromium (about 20% [1–3]), and this fact may explain the higher shear strength of adhesive bonds τnn for the coating of (Ti,Cr,Al)N. Meanwhile, the value of normal stresses Prn for the coating of (Ti,Cr,Al)N is noticeably lower in comparison with that for the coating of (Zr,Mo,Al)N, which in combination with the higher value of τnn leads to a less favorable value of fadh, especially in the temperature range of 600–700 °C. The indicated temperatures do not lead to any noticeable formation of a tribologically active oxide of Al_2O_3, the active formation of which starts at a temperature of 900 °C [41,63]. In contrast to the coatings with nanolayered structures considered above, the monolithic coating of ZrN exhibited a noticeable growth in τnn with an increase in temperature up to 700 °C and then the equally noticeable decrease in this parameter with a further increase in temperature. The coating of ZrN also exhibits a noticeable increase in its value of normal stresses P_{rn} with an increase in the temperature from 400 to 500 °C, which

may occur due to the thermal hardening of the coating. As a result, in the temperature range of 600–900 °C, the coating of ZrN has a lower value of fadh in comparison with the value of fadh for the coating of (Ti,Cr,Al)N.

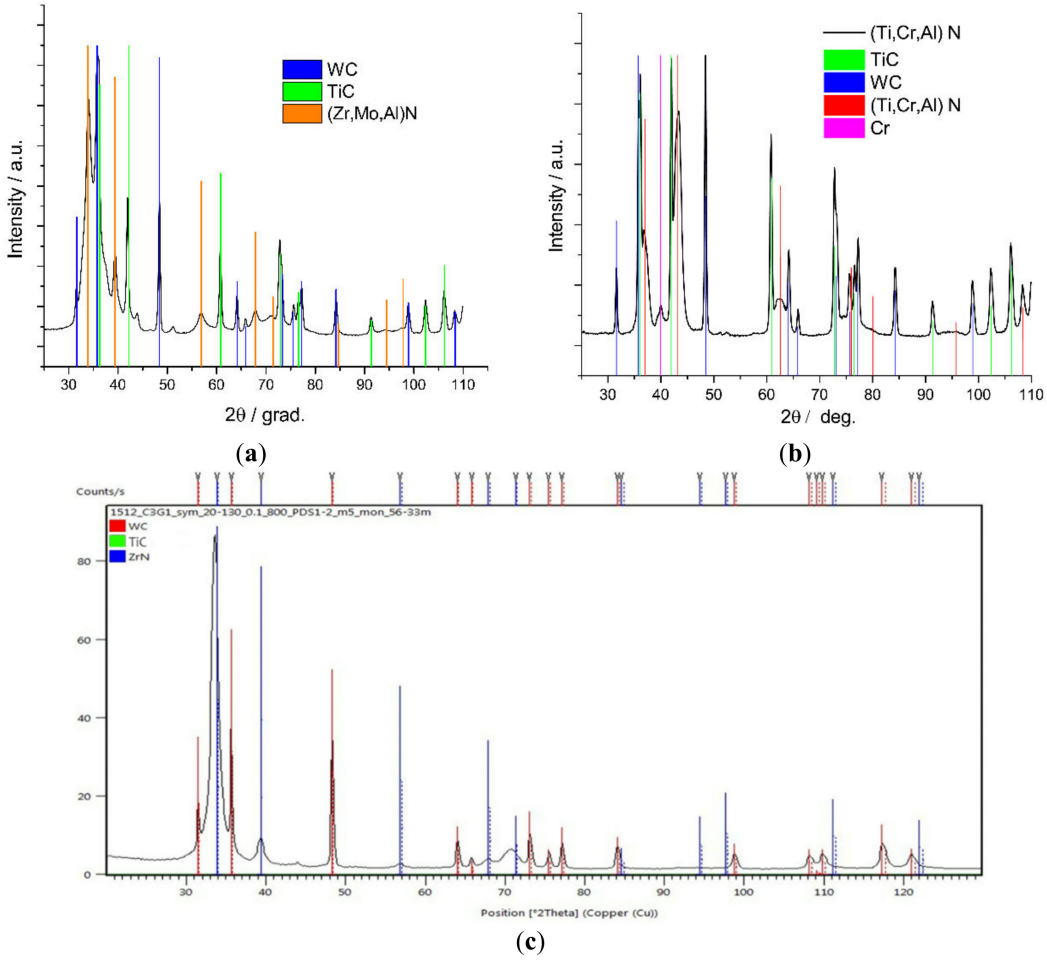

Figure 2. Investigation of the phase composition of the coatings, conducted by the X-ray diffraction (XRD) technique: (**a**) Zr-ZrN-(Zr,Mo,Al)N, (**b**) Ti-TiN-(Ti,Cr,Al)N, and (**c**) ZrN. The WC and TiC phases of the carbide substrate are also detected.

The flank wear rate for the coated cutting tools was studied during the tuning of Inconel 718, at two cutting speeds (v_c = 125 m/min and v_c = 200 m/min) (Figure 4). During the cutting at v_c = 125 m/min, all three coatings exhibited a noticeable increase in the tool life (for the uncoated tool, the tool life was only 6 min). The best wear resistance was detected for the cutting tool with the coating of (Zr,Mo,Al)N (the tool life reached 24 min), and the slightly shorter tool life was exhibited by the cutting tool with the coating of (Ti,Cr,Al)N (21 min). A considerably noticeable increase in the tool life at the considered cutting speed was also demonstrated by the cutting tool with the coating of ZrN (the tool life reached 15 min).

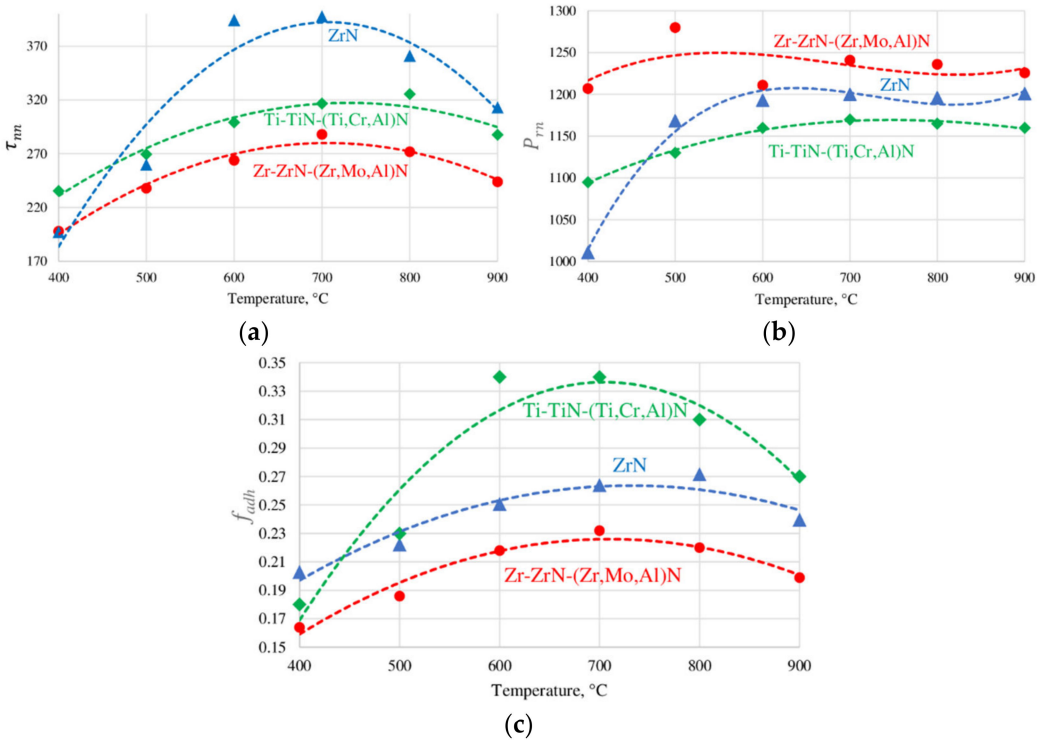

Figure 3. Investigation of the tribological properties of the coatings. (**a**) Shear strength of adhesive bonds τ_{nn}, (**b**) value of normal stresses P_{rn}, and (**c**) adhesive component of the COF f_{adh}.

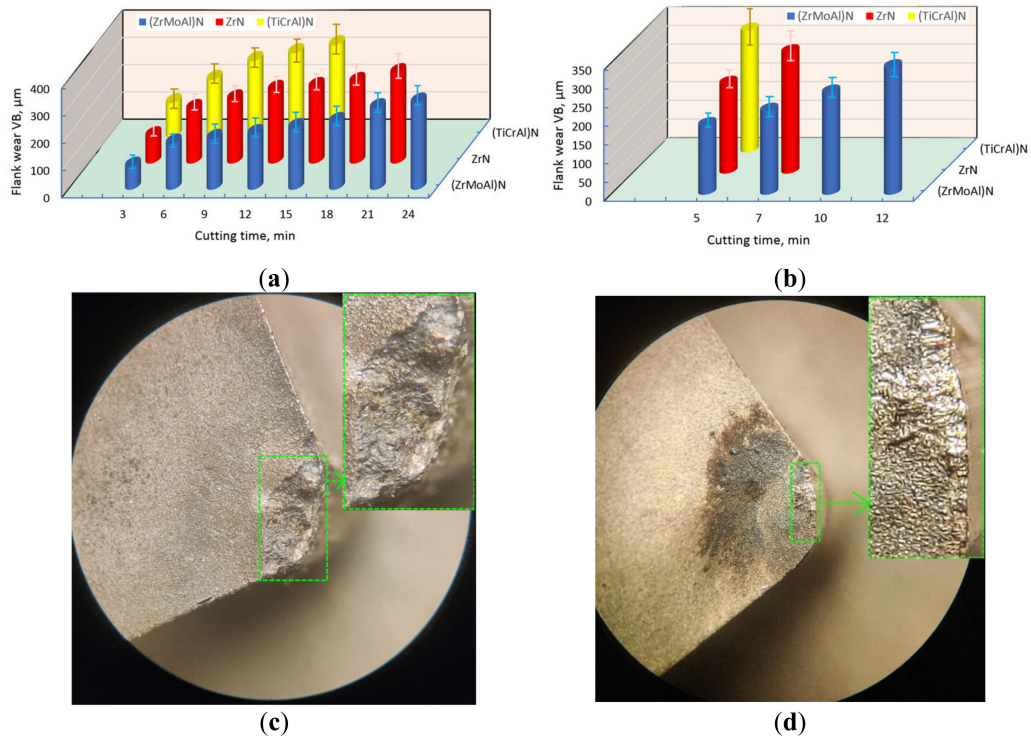

Figure 4. Relationship between the flank wear VB and the cutting time during the turning of Inconel 718 at various cutting speeds: (**a**) v_c = 125 m/min and (**b**) v_c = 200 m/min. View of the worn rake face of a tool coated with (**c**) (Ti,Cr,Al)N and (**d**) (Zr,Mo,Al)N, v_c = 200 m/min.

At the cutting speed of v_c = 200 m/min, the tool life of the uncoated tool was less than 5 min. At the same cutting speed, the longest tool life was also exhibited by the tool with the coating of (Zr,Mo,Al)N (12 min). Meanwhile, the tool lives of the tools with the

coatings of (Ti,Cr,Al)N and ZrN were considerably shorter (7 and 5 min, respectively). Therefore, the increase in the cutting speed from 125 to 200 m/min noticeably enhanced the differences in the wear resistance of the cutting tools with the different coatings under consideration [64–67].

Since the coating of (Zr,Mo,Al)N provided for the minimum value of the adhesion component of the COF fadh and the longest tool life at the cutting speeds of v_c = 125 m/min and especially v_c = 200 m/min (with the assumed dominance of the oxidation wear mechanism [18–20]), the mechanism of oxidation processes in the coating of (Zr,Mo,Al)N at various cutting speeds is considered in more detail.

4.2. Investigation of Oxidation Processes and Wear Pattern Typical for the (Zr,Mo,Al)N Coating during the Turning of Inconel 718

4.2.1. Oxidation Wear Pattern on the (Zr,Mo,Al)N Coating during the Turning of Inconel 718 at the Cutting Speed of v_c = 125 m/min

The analysis of the lamella cut out of the region adjacent to the wear crater on the rake face of the cutting tool reveals the presence of a zone of extensive delamination of the external coating layers (see Figure 5). The phase analysis of the delaminated fragment of the coating proves the presence of the main cubic phase of c-(Zr,Mo,Al)N and also an insignificant amount of the phase of c-(Mo,Zr,Al)N (solid solution of Zr and Al in MoN). The second cubic phase was not detected in the initial composition of the coating, which may be explained by the small amount of this phase or the lower accuracy of the XRD technique in comparison with the SAED method. It is also possible that this phase is being formed in the process of thermal action on the coating during the cutting. In addition to the nitride phases, the delaminated fragment of the coating also contains a considerably large amount of the oxide phase of ZrO_2, which is absent in the initial composition of the coating. No other possible oxide phases (oxides of molybdenum and aluminum) are formed, or they are formed in insignificant amounts.

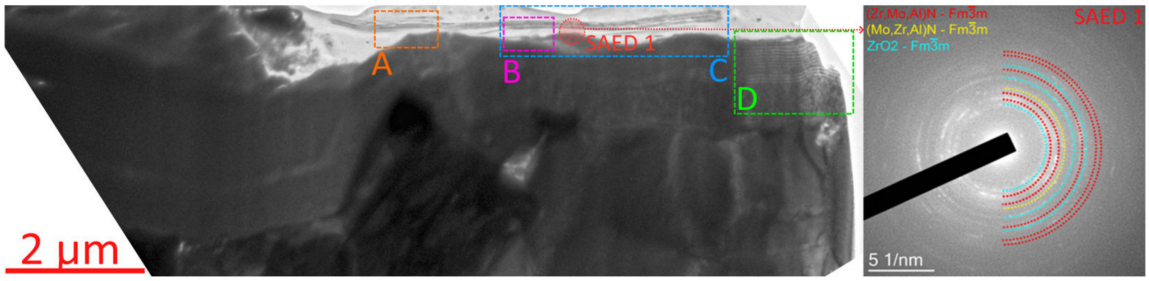

Figure 5. General view of the region, in which the wear pattern on the (Zr,Mo,Al)N coating was studied during the turning of Inconel 718 at the cutting speed of v_c = 125 m/min, after 24 min of cutting. Localization of the areas of detailed studies and the results of the SAED analysis focused on the phase composition of the oxidized area of the coating (SAED 1).

Figure 6 exhibits in detail the structure of the delaminated layers of the coating. The oxidation occurring under the influence of elevated temperatures results not only in delamination between the coating nanolayers but also in a typical arch deformation in separate sections of the coating nanolayers. These deformations can be associated both with the effect of temperature and with the noticeable difference in density between ZrN (7.09; 7.3 g/cm^3) and ZrO_2 (5.68 g/cm^3) [68].

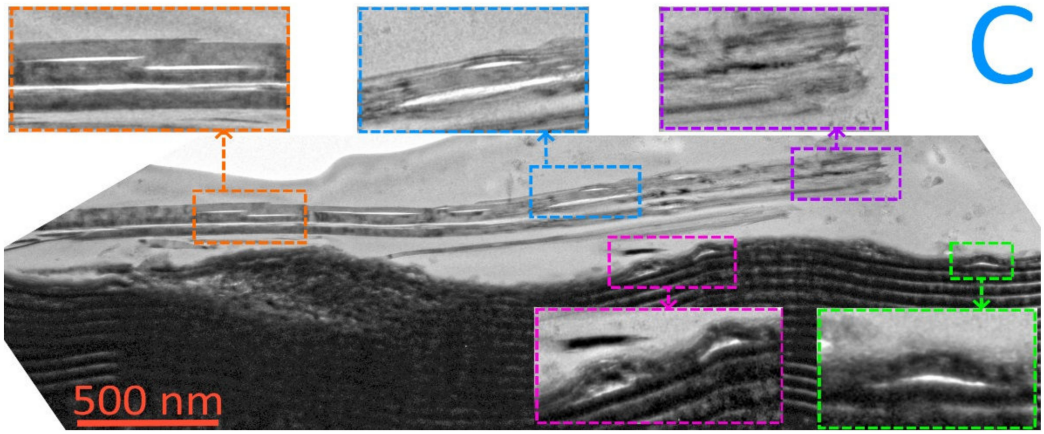

Figure 6. Analysis of the structure of oxidized layers in the (Zr,Mo,Al)N coating.

The examination of the external layers of the preserved part of the coating (Figure 7) (without taking into account the delaminated layers) reveals the presence of the phases similar to those found in the delaminated part of the coating (see Figure 5). There are cubic phases of c-(Zr,Mo,Al)N and c-(Mo,Zr,Al)N, as well as the oxide phase of ZrO_2. The EDX analysis of the chemical composition of the coating (Line L1) detects the diffusion of oxygen into the coating to the depth not exceeding 250 nm.

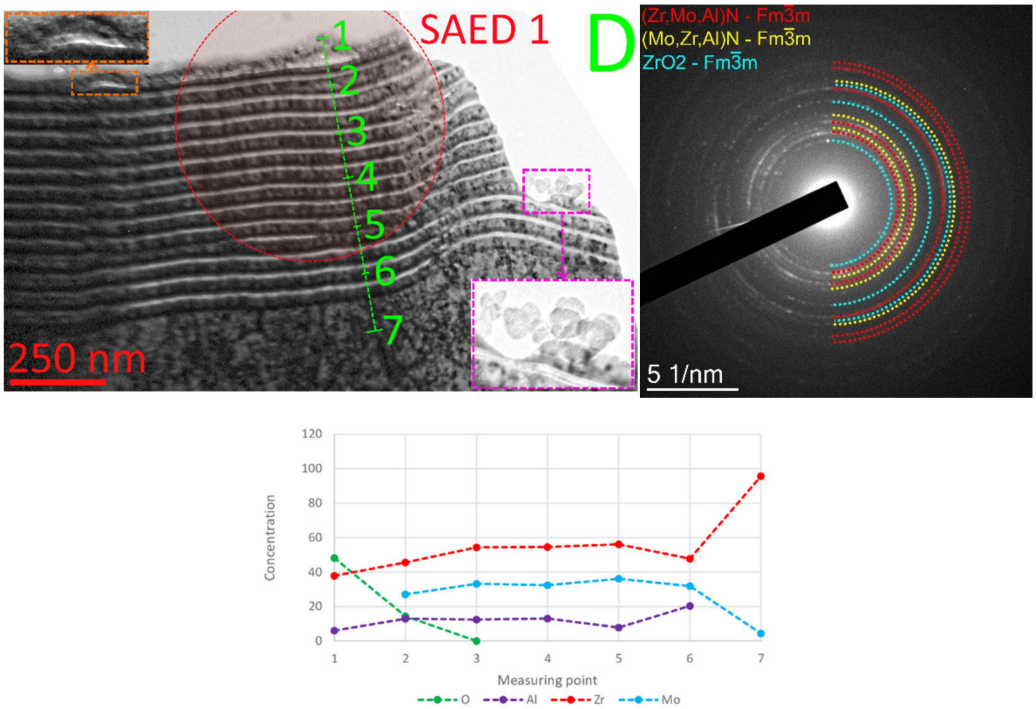

Figure 7. Oxidation processes in the worn area of the (Zr,Mo,Al)N coating. Localization of the study area D is exhibited in Figure 5.

The additional study of the depth to which oxygen diffuses into the structure of the coating in different sections (Figure 8) finds that the depth of oxygen diffusion reaches about 200–250 nm. Of the elements possibly diffusing from the material being machined into the coating structure, only a slight diffusion of iron is detected.

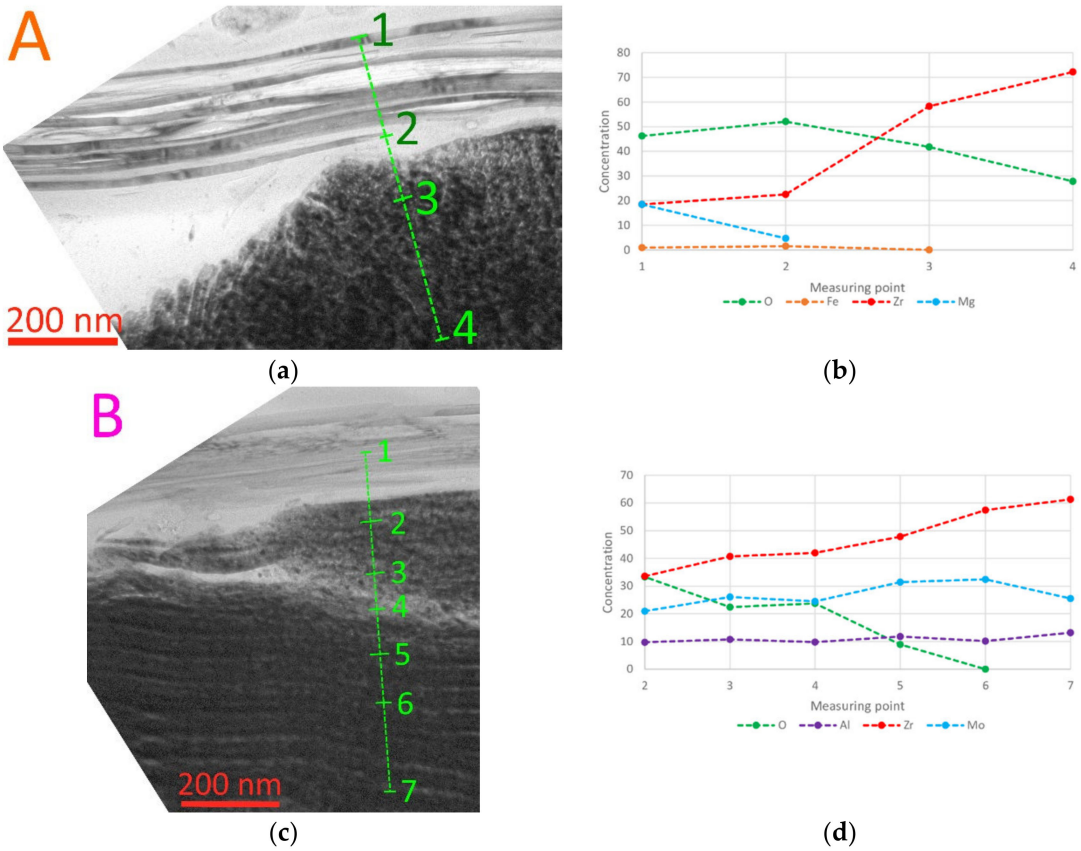

Figure 8. Investigation of the depth of oxygen diffusion into the structure of the (Zr,Mo,Al)N coating. Localization of the study areas A (**a**,**b**) and B (**c**,**d**) is exhibited in Figure 5.

4.2.2. Oxidation Wear Pattern on the (Zr,Mo,Al)N Coating during the Turning of Inconel 718 at the Cutting Speed of v_c = 200 m/min

The oxidation wear rate in the (Zr,Mo,Al)N coating at the cutting speed of v_c = 200 m/min differs considerably from the wear of the same coating at the cutting speed of v_c = 125 m/min. As is known, an increase in the cutting speed leads to a growth of temperature in the cutting zone [69,70]. As a result, an extensive zone of oxidation area is being formed in the coating. While at the cutting speed of v_c = 125 m/min, the oxidation damage is limited to a layer that is 200–250 nm thick, and then at the cutting speed of v_c = 200 m/min, the thickness of the oxidized layer exceeds 500 nm (see Figure 9). At the same time, the arch deformations, similar to those considered earlier, are detected.

The SAED analysis of the oxidized part of the coating detects almost complete oxidation. No initial cubic phases, but only oxide phases—oxides of zirconium ZrO_2 and molybdenum MoO_2—are detected (Figure 10). Oxide coatings (in particular, Al_2O_3, TiO_2, ZrO_2) have a beneficial effect on the cutting process, changing the tribological parameters in the cutting zone and reducing heat generation [71–73]. It should be noted that no oxides of molybdenum were detected in the worn areas of the coating after the machining at the cutting speed of v_c = 125 m/min.

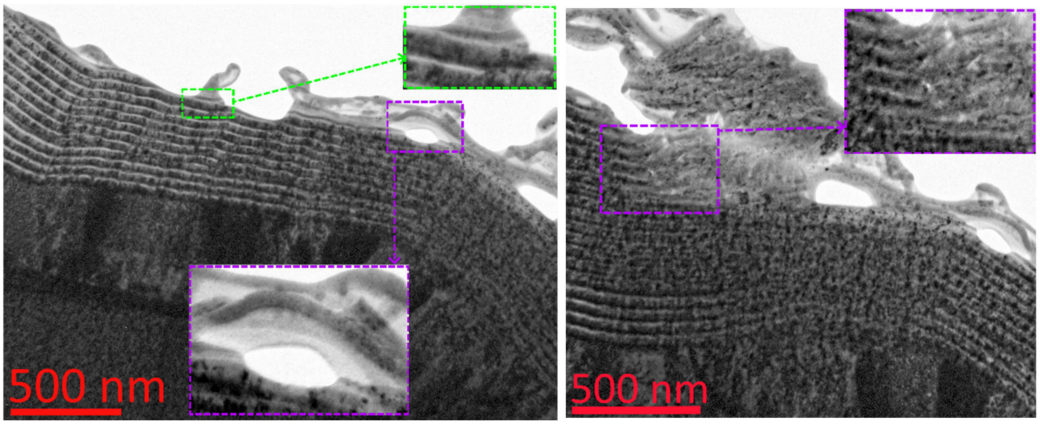

Figure 9. (**a**,**b**) Wear pattern on the (Zr,Mo,Al)N coating during the turning of Inconel 718 at the cutting speed of v_c = 200 m/min, after 12 min of cutting.

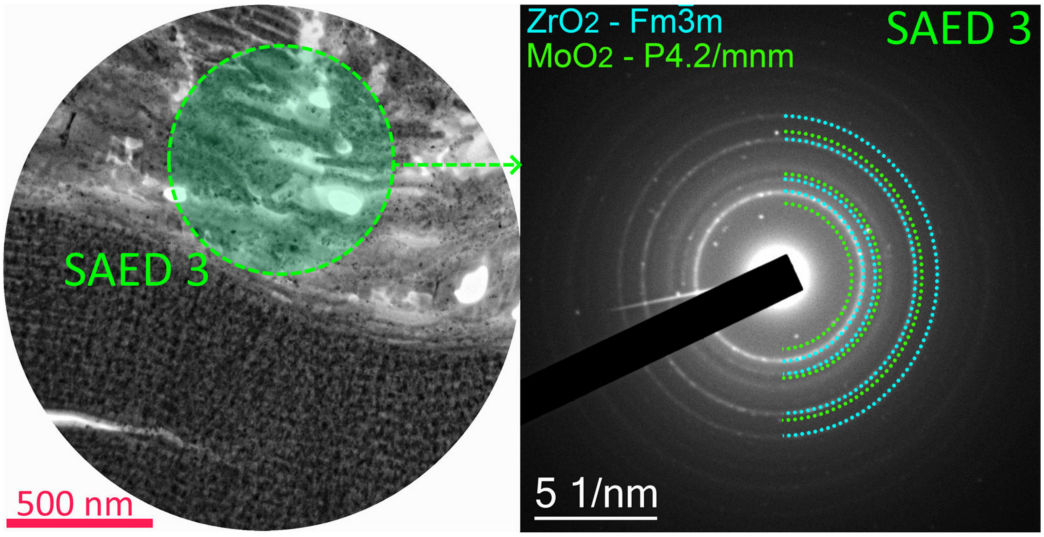

Figure 10. Analysis of the oxidation wear of the coating during the turning of Inconel 718 at the cutting speed of v_c = 200 m/min.

5. Conclusions

The properties and the oxidation wear patterns were studied for the composite nanostructured coating of Zr-ZrN-(Zr,Mo,Al)N during the turning of Inconel 718 alloy:

- The coating has a hardness of 32.3 ± 1.2 GPa, and its elastic modulus is 432.1 ± 21.4. The analysis of the phase composition of the coating with the XRD technique finds the presence of only one cubic nitride phase of c-(Zr,Mo,Al)N, but the study of the worn area of the coating with the SAED technique also reveals the presence of the second cubic phase of c-(Mo,Zr,Al)N.
- The comparison of the tribological properties of the (Zr,Mo,Al)N coating and the coatings of ZrN and (Ti,Cr,Al)N in contact with a cutting insert made of Inconel 718 exhibits a noticeably lower value of the adhesion component of the COF for the (Zr,Mo,Al)N coating, especially in the temperature range of 600–900 °C.
- The wear resistance of the cutting tools with the considered coatings during the turning of Inconel 718 was studied at the cutting speeds of v_c = 125 and 200 m/min. The coating of (Zr,Mo,Al)N provided for the best wear resistance of the tools at the cutting speed of v_c = 125 m/min (the tool life was four times longer in comparison with that of

the uncoated tool and 15% longer in comparison with the (Ti,Cr,Al)N-coated tool), and the wear resistance was significantly higher compared to that of the other considered coatings at the cutting speed of v_c = 200 m/min (the tool life was 2.5 times longer in comparison with that of the uncoated tool and 75% longer in comparison with that of the (Ti,Cr,Al)N-coated tool).

- While at the cutting speed of v_c = 125 m/min, the surface layers of the coating exhibit only partial oxidation of the external layers of the coating (to the depth not exceeding 250 nm), with considerably preserved cubic nitride phases, and then at the cutting speed of v_c = 200 m/min, almost complete oxidation of the coating (to the depth of at least 500 nm) occurs, accompanied with the decomposition of nitride phases. Meanwhile, the nanolayered structure of the coating stays partially preserved.

Author Contributions: Conceptualisation, A.V.; methodology, A.V. and F.M.; validation, A.M., M.M. (Mars Migranov) and A.T.; investigation, F.M., N.A. and M.M. (Mars Migranov) and M.M. (Maxim Mikhailov); resources, I.A.; data curation, M.M. (Mars Migranov) and M.M. (Maxim Mikhailov); writing—original draft preparation, A.V.; project administration, I.A.; funding acquisition, I.A. All authors have read and agreed to the published version of the manuscript.

Funding: Results of this work were obtained as part of the work under the agreement on the provision of subsidies dated 14 December 2020, no. 075-11-2020-032 (state contract identifier—000000S207520RNU0002) with the Ministry of Science and Higher Education of the Russian Federation.

Data Availability Statement: Data are available on request due to privacy or ethical restrictions.

Conflicts of Interest: The authors declare no conflict of interest.

References

1. Special Metals Corporation. INCONEL®Alloy 718. UNS N07718/W.Nr. 2.4668. Publication Number SMC-045. 2007. Available online: https://www.specialmetals.com/ (accessed on 3 September 2022).
2. What Are the Applications for Inconel 718? Langley Alloys. Available online: https://www.langleyalloys.com/knowledge-advice/what-are-the-applications-for-inconel-718 (accessed on 3 September 2022).
3. *NACE MR0175/ISO 15156-1:2001(E)*; NACE International: Houston, TX, USA, 2001.
4. Thakur, D.G.; Ramamoorthy, B.; Vijayaraghavan, L. Effect of posttreatments on the performance of tungsten carbide (K20) tool while machining (turning) of Inconel 718. *Int. J. Adv. Manuf. Technol.* **2015**, *76*, 587–596. [CrossRef]
5. Dudzinski, D.; Devillez, A.; Moufki, A.; Larrouquère, D.; Zerrouki, V.; Vigneau, J. A review of developments towards dry and machining (turning) of Inconel 718 alloy. *Int. J. Mach. Tools Manuf.* **2004**, *44*, 439–456. [CrossRef]
6. Arunachalam, R.; Mannan, M.A. Machinability of nickel-based high temperature alloys. *Mach. Sci. Technol.* **2000**, *4*, 127–168. [CrossRef]
7. Derrien, S.; Vigneau, J. High speed milling of difficult to machine alloys. In Proceedings of the First French and German Conference on High Speed Machining, University of Metz, Metz, France, 17–18 June 1997.
8. Jindal, P.C.; Santhanam, A.T.; Schleinkofer, U.; Shuster, A.F. Performance of PVD TiN, TiCN and TiAlN coated cemented carbide tools in turning. *Int. J. Refract. Hard Met.* **1999**, *17*, 163–170. [CrossRef]
9. Prengel, H.G.; Jindal, P.C.; Wendt, K.H.; Santhanam, A.T.; Hedge, P.L.; Penich, R.M. A new class of high performance PVD coatings for carbide cutting tools. *Surf. Coat. Technol.* **2001**, *139*, 25–34. [CrossRef]
10. Ducros, C.; Benevent, V.; Sanchette, F. Deposition, characterization and machining performance of multilayer PVD coatings on cemented carbide cutting tools. *Surf. Coat. Technol.* **2003**, *163-164*, 681–688. [CrossRef]
11. Mahesh, K.; Philip, J.T.; Joshi, S.N.; Kuriachen, B. Machinability of Inconel 718: A critical review on the impact of cutting temperatures. *Mater. Manuf. Process.* **2021**, *36*, 753–791. [CrossRef]
12. Hao, Z.-P.; Lu, Y.; Gao, D.; Fan, Y.-H.; Chang, Y.-L. Cutting Parameter Optimization Based on Optimal Cutting Temperature in Machining Inconel 718. *Mater. Manuf. Process.* **2012**, *27*, 1084–1089. [CrossRef]
13. Courbon, C.; Kramar, D.; Krajnik, P.; Pusavec, F.; Rech, J.; Kopac, J. Investigation of Machining Performance in High-Pressure Jet Assisted Turning of Inconel 718: An Experimental Study. *Int. J. Mach. Tools Manuf.* **2009**, *49*, 1114–1125. [CrossRef]
14. Thakur, D.G.; Ramamoorthy, B.; Vijayaraghavan, L. Some Investigations on High Speed Dry Machining of Aerospace Material Inconel 718 Using Multicoated Carbide Inserts. *Mater. Manuf. Process.* **2012**, *27*, 1066–1072. [CrossRef]
15. Zhao, J.; Liu, Z.; Shen, Q.; Wang, B.; Wang, Q. Investigation of Cutting Temperature during Turning Inconel 718 with (Ti,Al)N PVD Coated Cemented Carbide Tools. *Materials* **2018**, *11*, 1281. [CrossRef]
16. Fan, Y.H.; Hao, Z.P.; Lin, J.Q.; Yu, Z.X. Material Response at Tool–Chip Interface and Its Effects on Tool Wear in Turning Inconel 718. *Mater. Manuf. Process.* **2014**, *29*, 1446–1452. [CrossRef]

17. Ezugwu, E.O.; Bonney, J. Effect of High-Pressure Coolant Supply When Machining Nickel-Base, Inconel 718, Alloy with Coated Carbide Tools. *J. Mater. Process. Technol.* **2004**, *153–154*, 1045–1050. [CrossRef]
18. Itakura, K.; Kuroda, M.; Omokawa, H.; Itani, H.; Yamamoto, K.; Ariura, Y. Wear mechanism of coated cemented carbide tool in coated tool in cutting of Inconel 718 super-heat resisting alloy. *Int. J. Jpn. Soc. Precis. Eng.* **1999**, *33*, 326–333.
19. Chandra Behera, B.; Sudarsan Ghosh, C.; Paruchuri, V.R. Study of Saw-Tooth Chip in Machining of Inconel 718 by Metallographic Technique. *Mach. Sci. Technol.* **2019**, *23*, 431–454. [CrossRef]
20. Hua, Y.; Liu, Z. Effects of Cutting Parameters and Tool Nose Radius on Surface Roughness and Work Hardening during Dry Turning Inconel 718. *Int. J. Adv. Manuf. Technol.* **2018**, *96*, 2421–2430. [CrossRef]
21. Alaudin, M.; El Baradie, M.A.; Hashmi, M.S.J. Tool life testing in the end milling of Inconel 718. *J. Mater. Process Technol.* **1995**, *55*, 321–330. [CrossRef]
22. Zhao, Y.; Feng, K.; Yao, C.; Li, Z. Effect of MoO_3 on the microstructure and tribological properties of laser-clad Ni60/nanoCu/h-BN/MoO3 composite coatings over wide temperature range. *Surf. Coat. Technol.* **2020**, *387*, 125477. [CrossRef]
23. Tao, H.; Tsai, M.T.; Chen, H.W.; Huang, J.C.; Duh, J.G. Improving high-temperature tribological characteristics on nanocomposite CrAlSiN coating by Mo doping. *Surf. Coat. Technol.* **2018**, *349*, 752–756. [CrossRef]
24. Koshy, R.A.; Graham, M.E.; Marks, L.D. Temperature activated self-lubrication in CrN/Mo_2N nanolayer coatings. *Surf. Coat. Technol.* **2010**, *204*, 1359–1365. [CrossRef]
25. Vetter, J.; Eriksson, A.O.; Reiter, A.; Derflinger, V.; Kalss, W. Quo vadis: Alcr-based coatings in industrial applications. *Coatings* **2021**, *11*, 344. [CrossRef]
26. Fox-Rabinovich, G.S.; Yamamoto, K.; Veldhuis, S.C.; Kovalev, A.I.; Dosbaeva, G.K. Tribological adaptability of TiAlCrN PVD coatings under high performance dry machining conditions. *Surf. Coat. Technol.* **2005**, *200*, 1804–1813. [CrossRef]
27. Grigoriev, S.; Vereschaka, A.; Milovich, F.; Tabakov, V.; Sitnikov, N.; Andreev, N.; Sviridova, T.; Bublikov, J. Investigation of multicomponent nanolayer coatings based on nitrides of Cr, Mo, Zr, Nb, and Al. *Surf. Coat. Technol.* **2020**, *401*, 126258. [CrossRef]
28. Grigoriev, S.; Vereschaka, A.; Milovich, F.; Sitnikov, N.; Andreev, N.; Bublikov, J.; Kutina, N. Investigation of the properties of the Cr,Mo-(Cr,Mo,Zr,Nb)N-(Cr,Mo,Zr,Nb,Al)N multilayer composite multicomponent coating with nanostructured wear-resistant layer. *Wear* **2021**, *468–469*, 203597. [CrossRef]
29. Vereschaka, A.; Tabakov, V.; Grigoriev, S.; Sitnikov, N.; Oganyan, G.; Andreev, N.; Milovich, F. Investigation of wear dynamics for cutting tools with multilayer composite nanostructured coatings in turning constructional steel. *Wear* **2019**, *420–421*, 17–37. [CrossRef]
30. Vereschaka, A.; Tabakov, V.; Grigoriev, S.; Aksenenko, A.; Sitnikov, N.; Oganyan, G.; Seleznev, A.; Shevchenko, S. Effect of adhesion and the wear-resistant layer thickness ratio on mechanical and performance properties of ZrN-(Zr,Al,Si)N coatings. *Surf. Coat. Technol.* **2019**, *357*, 218–23424. [CrossRef]
31. Vereschaka, A.; Tabakov, V.; Grigoriev, S.; Sitnikov, N.; Milovich, F.; Andreev, N.; Sotova, C.; Kutina, N. Investigation of the influence of the thickness of nanolayers in wear-resistant layers of Ti-TiN-(Ti,Cr,Al)N coating on destruction in the cutting and wear of carbide cutting tools. *Surf. Coat. Technol.* **2020**, *385*, 125402. [CrossRef]
32. Volosova, M.A.; Grigor'ev, S.N.; Kuzin, V.V. Effect of Titanium Nitride Coating on Stress Structural Inhomogeneity in Oxide-Carbide Ceramic. Part 4. Action of Heat Flow. *Refract. Ind. Ceram.* **2015**, *56*, 91–96. [CrossRef]
33. Grigoriev, S.N.; Vereschaka, A.A.; Fyodorov, S.V.; Sitnikov, N.N.; Batako, A.D. Comparative analysis of cutting properties and nature of wear of carbide cutting tools with multi-layered nano-structured and gradient coatings produced by using of various deposition methods. *Int. J. Adv. Manuf. Technol.* **2017**, *90*, 3421–3435. [CrossRef]
34. Lamni, R.; Sanjinés, R.; Parlinska-Wojtan, M.; Karimi, A.; Lévy, F. Microstructure and nanohardness properties of Zr–Al–N and Zr–Cr–N thin films. *J. Vac. Sci. Technol. A* **2005**, *23*, 593. [CrossRef]
35. Kong, J.-Z.; Hou, T.-J.; Wang, Q.-Z.; Yin, L.; Zhou, F.; Zhou, Z.-F.; Li, L.K.-Y. Influence of titanium or aluminum doping on the electrochemical properties of CrN coatings in artificial seawater. *Surf. Coat. Technol.* **2016**, *307*, 118–124. [CrossRef]
36. Wang, Q.Z.; Zhou, F.; Yan, J.W. Evaluating mechanical properties and crack resistance of CrN, CrTiN, CrAlN and CrTiAlN coatings by nanoindentation and scratch tests. *Surf. Coat. Technol.* **2016**, *285*, 203–213. [CrossRef]
37. Beliardouh, N.E.; Bouzid, K.; Nouveau, C.; Tlili, B.; Walock, M.J. Tribological and electrochemical performances of Cr/CrN and Cr/CrN/CrAlN multilayer coatings deposited by RF magnetron sputtering. *Tribol. Int.* **2015**, *82*, 443–452. [CrossRef]
38. Rogström, L.; Johansson, M.P.; Ghafoor, N.; Hultman, L.; Odén, M. Influence of chemical composition and deposition conditions on microstructure evolution during annealing of arc evaporated ZrAlN thin films. *J. Vac. Sci. Technol. A* **2012**, *30*, 031504. [CrossRef]
39. Rogström, L.; Ghafoor, N.; Schroeder, J.; Schell, N.; Birch, J.; Ahlgren, M.; Odén, M. Thermal stability of wurtzite Zr1–xAlxN coatings studied by in situ high-energy X-ray diffraction during annealing. *J. Appl. Phys.* **2015**, *118*, 035309. [CrossRef]
40. Holec, D.; Rachbauer, R.; Chen, L.; Wang, L.; Luef, D.; Mayrhofer, P.H. Phase stability and alloy-related trends in Ti–Al–N, Zr–Al–N and Hf–Al–N systems from first principles. *Surf. Coat. Technol.* **2011**, *206*, 1698–1704. [CrossRef]
41. Grigoriev, S.; Vereschaka, A.; Uglov, V.; Milovich, F.; Cherenda, N.; Andreev, N.; Migranov, M.; Seleznev, A. Influence of tribological properties of Zr-ZrN-(Zr,Cr,Al)N and Zr-ZrN-(Zr,Mo,Al)N multilayer nanostructured coatings on the cutting properties of coated tools during dry turning of Inconel 718 alloy. *Wear* **2023**, *512-513*, 204521. [CrossRef]
42. Ghafoor, N.; Johnson, L.; Klenov, D.; Demeulemeester, J.; Desjardins, P.; Petrov, I.; Hultman, L.; Odén, M. Nanolabyrinthine ZrAlN thin films by self-organization of interwoven single-crystal cubic and hexagonal phases. *APL Mater.* **2013**, *1*, 022105. [CrossRef]

43. Mayrhofer, P.H.; Sonnleitner, D.; Bartosik, M.; Holec, D. Structural and mechanical evolution of reactively and non-reactively sputtered Zr–Al–N thin films during annealing. *Surf. Coat. Technol.* **2014**, *244*, 52–56. [CrossRef]
44. Franz, R.; Lechthaler, M.; Polzer, C.; Mitterer, C. Oxidation behaviour and tribological properties of arc-evaporated ZrAlN hard coatings. *Surf. Coat. Technol.* **2012**, *206*, 2337–2345. [CrossRef]
45. Suna, J.; Musil, J.; Dohnal, P. Control of macrostress s in reactively sputtered Mo–Al–N films by total gas pressure. *Vacuum* **2006**, *80*, 588–592. [CrossRef]
46. Xu, J.; Ju, H.; Yu, L. Microstructure, oxidation resistance, mechanical and tribological properties of Mo-Al-N films by reactive magnetron sputtering. *Vacuum* **2014**, *103*, 21–27. [CrossRef]
47. Klimashin, F.F.; Euchner, H.; Mayrhofer, P.H. Computational and experimental studies on structure and mechanical properties of Mo-Al-N. *Acta Mater.* **2016**, *107*, 273–278. [CrossRef]
48. Yang, J.F.; Yuan, Z.G.; Liu, Q.; Wang, X.P.; Fang, Q.F. Characterization of Mo–Al–N nanocrystalline films synthesized by reactive magnetron sputtering. *Mater. Res. Bull.* **2009**, *44*, 86–90. [CrossRef]
49. Tomaszewski, Ł.; Gulbinski, W.; Urbanowicz, A.; Suszko, T.; Lewandowski, A.; Gulbinski, W. TiAlN based wear resistant coatings modified by molybdenum addition. *Vacuum* **2015**, *121*, 223–229. [CrossRef]
50. Yousaf, M.I.; Pelenovicha, V.O.; Yangc, B.; Liua, C.S.; Fu, D.J. Effect of bilayer period on structural and mechanical properties of nanocomposite TiAlN/MoN multilayer films synthesized by cathodic arc ion-plating. *Surf. Coat. Technol.* **2015**, *282*, 94–102. [CrossRef]
51. Bobzina, K.; Brögelmanna, T.; Kalscheuera, C.; Stahlb, K.; Lohnerb, T.; Yilmaz, M. (Cr,Al)N and (Cr,Al,Mo)N hard coatings for tribological applications under minimum quantity lubrication. *Tribol Int.* **2019**, *140*, 105817. [CrossRef]
52. Gilewicz, A.; Warcholinski, B. Deposition and characterisation of Mo2N/CrN multilayer coatings prepared by cathodic arc evaporation. *Surf. Coat. Technol.* **2015**, *279*, 126–133. [CrossRef]
53. Jua, H.; Yua, D.; Xua, J.; Yua, L.; Zuoa, B.; Genga, Y.; Huanga, T.; Shaod, L.; Renb, L.; Dub, C.; et al. Crystal structure and tribological properties of Zr-Al-Mo-N composite films deposited by magnetron sputtering. *Mater. Chem. Phys.* **2019**, *230*, 347–354. [CrossRef]
54. Rogström, L.; Johansson-Jõesaar, M.P.; Landälv, L.; Ahlgren, M.; Odén, M. Wear behavior of ZrAlN coated cutting tools during turning. *Surf. Coat. Technol.* **2015**, *282*, 180–187. [CrossRef]
55. Vereschaka, A.; Grigoriev, S.; Milovich, F.; Sitnikov, N.; Migranov, M.; Andreev, N.; Bublikov, J.; Sotova, C. Investigation of tribological and functional properties of Cr,Mo-(Cr,Mo)N-(Cr,Mo,Al)N multilayer composite coating. *Tribol. Int.* **2021**, *155*, 106804. [CrossRef]
56. Vereschaka, A.; Milovich, F.; Migranov, M.; Andreev, N.; Alexandrov, I.; Muranov, A.; Mikhailov, M.; Tatarkanov, A. Investigation of the tribological and operational properties of $(Me_x,Mo_y,Al_{1-(x+y)})N$ (Me–Ti, Zr or Cr) coatings. *Tribol. Int.* **2022**, *165*, 107305. [CrossRef]
57. Grigoriev, S.; Vereschaka, A.; Milovich, F.; Migranov, M.; Andreev, N.; Bublikov, J.; Sitnikov, N.; Oganyan, G. Investigation of the tribological properties of Ti-TiN-(Ti,Al,Nb,Zr)N composite coating and its efficiency in increasing wear resistance of metal cutting tools. *Tribol. Int.* **2021**, *164*, 107236. [CrossRef]
58. Grigoriev, S.; Vereschaka, A.; Milovich, F.; Andreev, N.; Bublikov, J.; Seleznev, A.; Kutina, N. Influence of Mo content on the properties of multilayer nanostructured coatings based on the (Mo,Cr,Al)N system. *Tribol. Int.* **2022**, *174*, 107741. [CrossRef]
59. Vereschaka, A.A.; Grigoriev, S.N. Study of cracking mechanisms in multi-layered composite nano-structured coatings. *Wear* **2017**, *378–379*, 43–57. [CrossRef]
60. Grigoriev, S.; Vereschaka, A.; Zelenkov, V.; Sitnikov, N.; Bublikov, J.; Milovich, F.; Andreev, N.; Mustafaev, E. Specific features of the structure and properties of arc-PVD coatings depending on the spatial arrangement of the sample in the chamber. *Vacuum* **2022**, *200*, 111047. [CrossRef]
61. Grigoriev, S.; Vereschaka, A.; Zelenkov, V.; Sitnikov, N.; Bublikov, J.; Milovich, F.; Andreev, N.; Sotova, C. Investigation of the influence of the features of the deposition process on the structural features of microparticles in PVD coatings. *Vacuum* **2022**, *202*, 111144. [CrossRef]
62. Shuster, L.S.; Migranov, M.S. Device for Investigating Adhesion Interaction. Russia Patent 34249, 26 March 2003.
63. Prescott, R.; Graham, M.J. The formation of aluminum oxide scales on high-temperature alloys. *Oxid. Met.* **1992**, *38*, 233–254. [CrossRef]
64. Özbek, N.A.; Özbek, O.; Kara, F. Statistical Analysis of the Effect of the Cutting Tool Coating Type on Sustainable Machining Parameters. *J. Mater. Eng. Perform.* **2021**, *30*, 7783–7795. [CrossRef]
65. Dabees, S.; Mirzaei, S.; Kaspar, P.; Holcman, V.; Sobola, D. Characterization and Evaluation of Engineered Coating Techniques for Different Cutting Tools—Review. *Materials* **2022**, *15*, 5633. [CrossRef]
66. Fox-Rabinovich, G.; Gershman, I.S.; Yamamoto, K.; Dosbaeva, J.; Veldhuis, S. Effect of the adaptive response on the wear behavior of pvd and cvd coated cutting tools during machining with built up edge formation. *Nanomaterials* **2020**, *10*, 2489. [CrossRef] [PubMed]
67. Özbek, O.; Saruhan, H. The effect of vibration and cutting zone temperature on surface roughness and tool wear in eco-friendly MQL turning of AISI D2. *J. Mater. Res. Technol.* **2020**, *9*, 2762–2772. [CrossRef]
68. Nielsen, R. Zirconium and Zirconium Compounds. In *Ullmann's Encyclopedia of Industrial Chemistry*; Wiley-VCH: Weinheim, Germany, 2005.

69. Su, G.; Xiao, X.; Du, J.; Zhang, J.; Zhang, P.; Liu, Z.; Xu, C. On cutting temperatures in high and ultrahigh-speed machining. *Int. J. Adv. Manuf. Technol.* **2020**, *107*, 73–83. [CrossRef]
70. Longbottom, J.M.; Lanham, J.D. A review of research related to Salomon's hypothesis on cutting speeds and temperatures. *Int. J. Mach. Tools Manuf.* **2006**, *46*, 1740–1747. [CrossRef]
71. Zhou, F.; Deng, C.; Wang, Y.; Liu, M.; Wang, L.; Wang, Y.; Zhang, X. Characterization of multi-scale synergistic toughened nanostructured YSZ thermal barrier coatings: From feedstocks to coatings. *J. Eur. Ceram. Soc.* **2020**, *40*, 1443–1452. [CrossRef]
72. Yu, J.; Wang, Y.; Zhou, F.; Wang, L.; Pan, Z. Laser remelting of plasma-sprayed nanostructured Al_2 O_3–20 wt.% ZrO_2 coatings onto 316L stainless steel. *Appl. Surf. Sci.* **2018**, *431*, 112–121. [CrossRef]
73. Zou, Z.; Wang, Y.; Zhou, F.; Wang, L.; Liu, S.; Wang, Y. Tribological property of plasma-sprayed Al_2 O_3-13wt%TiO_2 coatings onto resin-based composites. *Appl. Surf. Sci.* **2018**, *431*, 75–80. [CrossRef]